



HAL
open science

Intelligent Reflecting Surface Assisted mmWave Integrated Sensing and Communication Systems

Zhengyu Zhu, Zheng Li, Zheng Chu, Yingying Guan, Qingqing Wu, Pei Xiao,
Marco Di Renzo, Inkyu Lee

► **To cite this version:**

Zhengyu Zhu, Zheng Li, Zheng Chu, Yingying Guan, Qingqing Wu, et al.. Intelligent Reflecting Surface Assisted mmWave Integrated Sensing and Communication Systems. IEEE Internet of Things Journal, 2024, 11 (18), pp.29427 - 29437. hal-04733298

HAL Id: hal-04733298

<https://hal.science/hal-04733298v1>

Submitted on 20 Oct 2024

HAL is a multi-disciplinary open access archive for the deposit and dissemination of scientific research documents, whether they are published or not. The documents may come from teaching and research institutions in France or abroad, or from public or private research centers.

L'archive ouverte pluridisciplinaire **HAL**, est destinée au dépôt et à la diffusion de documents scientifiques de niveau recherche, publiés ou non, émanant des établissements d'enseignement et de recherche français ou étrangers, des laboratoires publics ou privés.

Intelligent Reflecting Surface Assisted mmWave Integrated Sensing and Communication Systems

Zhengyu Zhu, *Senior Member, IEEE*, Zheng Li, Zheng Chu, Yingying Guan, Qingqing Wu, *Senior Member, IEEE*, Pei Xiao, *Senior Member, IEEE*, Marco Di Renzo, *Fellow, IEEE*, and Inkyu Lee, *Fellow, IEEE*

Abstract—This paper proposes an intelligent reflecting surface (IRS) assisted integrated sensing and communication (ISAC) system operating in the millimeter-wave band. Specifically, the ISAC system consists of a radar subsystem and a communication subsystem to detect multiple targets and communicate with the users simultaneously. The IRS is used to configure the radio propagation environment by changing the phase of the radio signal to enhance the communication transmission rate. In the proposed scheme, we first derive a closed-form solution for the radar signal covariance matrix to generate a radar beam pattern in the angle of interest. Then, we jointly optimize the beamforming vector of the communication subsystem and the IRS phase shifts to enhance the communication transmission rate. To decouple the multiple variables to be optimized, the alternating optimization and quadratic transformation methods are applied to determine the communication beamforming vector and the IRS phase shifts. Specifically, we utilize the majorization minimization and the complex circle manifold methods to compute the IRS phase shifts. Simulation results verify the effectiveness of the

proposed algorithm and demonstrate that an IRS can improve the performance of ISAC systems.

Index Terms—Integrated sensing and communication, intelligent reflecting surface, performance tradeoff, waveform design, MIMO radar.

I. INTRODUCTION

In recent years, due to the similarity between radar and communication in terms of hardware components and signal processing algorithms, as well as the scarcity of spectrum resources, integrated sensing and communication (ISAC) has emerged as one of the key technologies for 6G [1]–[3]. The sensing function collects and extracts useful information from noisy observations, and the communication function is intended to transmit information through specialized signals and recover the transmitted information from noisy received signals. In terms of hardware, ISAC is intended to integrate these two functions aiming for a trade-off between them, which is expected to significantly improve the spectral and energy efficiencies and to reduce the cost of the hardware as well. In terms of applications, ISAC can provide users with high-quality communication performance while providing high-precision sensing performance in terms of target detection. In general, ISAC has broad application prospects in areas such as smart home, smart transportation and smart medical care [4].

However, the integration of sensing into a communication system requires an appropriate allocation of the available resources. Also, it may lead to severe interference between sensing and communication, which may degrade the communication performance [5]. To tackle the problem, intelligent reflecting surfaces (IRS), a low-cost information transmission technology, constitutes a promising approach to facilitate the integration of sensing and communication [6]–[10]. Notably, IRS allows bypassing obstacles, by dynamically creating smart reflections beyond the conventional law of reflection [11]–[15], which is especially beneficial for communication in high frequency bands, such as the millimeter-wave (mmWave) spectrum. Motivated by these considerations, in this paper, we analyze IRS-aided ISAC systems in mmWave networks.

In [15], the authors studied IRS-assisted multiple-input single-output radio systems with multiple backscatter devices, and they proposed a block coordinate descent algorithm based on Dinkelbach’s method to obtain a suboptimal solution, which improves more than two times the system energy efficiency compared with conventional algorithms. The application of

This work of Zhengyu Zhu was supported in part by Program for Science & Technology Innovation Talents in Universities of Henan Province under Grant 23HASTIT019, in part by Natural Science Foundation of Henan Province under Grant 232300421097, in part by State Key Laboratory of Integrated Services Networks under Grant ISN25-24, Xidian University; The work of M. Di Renzo was supported in part by the European Commission through the Horizon Europe project titled COVER under grant agreement number 101086228, the Horizon Europe project titled UNITE under grant agreement number 101129618, and the Horizon Europe project titled INSTINCT under grant agreement number 101139161, as well as by the Agence Nationale de la Recherche (ANR) through the France 2030 project titled ANR-PEPR Networks of the Future under grant agreement NF-YACARI 22-PEFT-0005, and by the CHIST-ERA project titled PASSIONATE under grant agreement CHIST-ERA-22-WAI-04 through ANR-23-CHR4-0003-01. (Corresponding author: Zheng Chu and Inkyu Lee)

Z. Zhu and Z. Li are with the School of Electrical and Information Engineering, Zhengzhou University, Zhengzhou, 450001, China, and Z. Zhu is also with State Key Laboratory of Integrated Services Networks, Xidian University, Xi’an, 710071, China. (e-mail: zhuzhengyu6@gmail.com, stones_li@outlook.com).

Z. Chu is with the Department of Electrical and Electronic Engineering, University of Nottingham Ningbo China, Ningbo 315100, China, and also with the Next-Generation Internet of Everything Laboratory, University of Nottingham Ningbo China, Ningbo 315100, China. (e-mail: andrew.chuzheng7@gmail.com).

Y. Guan is with the School of Computer Science and Engineering, Northeastern University, Shenyang 110819, China. (e-mail: yingying-guan@foxmail.com).

Qingqing Wu is with the Department of Electronic Engineering, Shanghai Jiao Tong University, Shanghai 201210, China. (e-mail: qingqingwu@sjtu.edu.cn).

P. Xiao is with the 5GIC & 6GIC, Institute for Communication Systems (ICS), University of Surrey, Guildford GU2 7XH, UK. (e-mail: p.xiao@surrey.ac.uk).

M. Di Renzo is with Université Paris-Saclay, CNRS, CentraleSupélec, Laboratoire des Signaux et Systèmes, 3 Rue Joliot-Curie, 91192 Gif-sur-Yvette, France. (e-mail: marco.di-renzo@universite-paris-saclay.fr).

I. Lee is with the School of Electrical Engineering, Korea University, Seoul, Korea. (e-mail: inkyu@korea.ac.kr).

IRS to enhance the physical layer security in communication systems is analyzed in [16]–[18]. In non-orthogonal multiple access wireless systems, in addition, IRS has demonstrated major advantages in interference management, coverage enhancement, energy efficiency and spectrum efficiency [19]–[22].

The authors of [23] proposed two distinct deployment strategies for radar and communication: separated deployment and shared deployment. In the separated deployment, the radar signal is designed to occupy the null space of the downlink communication channel. In the shared deployment, on the other hand, the beamforming is optimized to satisfy the performance requirements of both radar and communication functions. In [24], an integrated communication and radar system is considered, where a base station (BS) and a multiple-input multiple-output (MIMO) radar are combined, to simultaneously provide communication services and detect multiple targets. The authors investigated the integration of active and nearly passive beamforming techniques in IRS-assisted radar and communication systems to mitigate multiuser interference [25]. Aerial IRS for improving the security in ISAC systems is investigated in [26]. Therein, the authors analyzed the performance of secure transmission in jamming environments by optimizing the deployment of IRS over the air. Due to the blockage of the direct communication link, a distributed semi-passive IRS is deployed in [27] for location sensing and data transmission. Simulation results showed that the deployment of IRS can enable position-sensing solutions offering millimeter-level accuracy. Interested readers are referred to the recent comprehensive survey on IRS for ISAC in [28], for more information on the state of research in this field.

In this paper, we investigate an IRS-aided ISAC system in an mmWave multi-user downlink scenario. The main contributions of this paper are summarized as follows:

- In an IRS-assisted ISAC system in the mmWave band, the radar subsystem is used to sense the targets of interest, while the communication subsystem provides high-speed communication services to users. The IRS is deployed to simplify the design of BS beamforming and consequently to improve the performance of the communication subsystem.
- We consider the problem of minimizing the beampattern error between the designed and desired beampatterns while maximizing the sum transmission rate, subject to constraints on the communication beamforming vector and the IRS phase shifts. The tight coupling among the optimization variables makes the formulated problem non-convex. To tackle this problem and develop a computationally efficient solution, we decompose the original problem into two sub-problems that can be solved separately.
- Since the desired radar beampattern is influenced by the radar signal covariance (RSC) matrix, we compute a closed-form solution for the RSC matrix by relaxing certain constraints in the first sub-problem. Additionally, the quadratic transformation (QT) technique is adopted for the second sub-problem. The alternating optimization (AO) algorithm is utilized to obtain efficient solutions

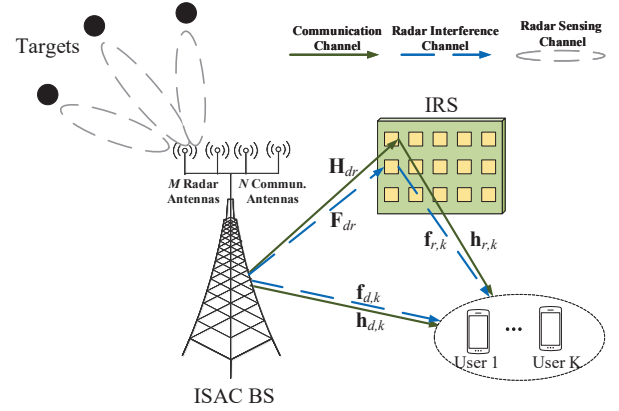


Fig. 1. The considered IRS-assisted ISAC system.

for the beamforming vector and the phase shifts of the IRS. Specifically, the phase shifts of the IRS are obtained by the majorization minimization (MM) and the complex circle manifold (CCM) algorithms.

The remainder of the paper is organized as follows: We introduce the system model in Section II. The proposed solutions are presented in Section III. We illustrate the numerical results in Section IV and conclude the paper in Section V.

Notations: Uppercase boldface and lowercase boldface symbols denote vectors and matrices, respectively. The notation $\mathbf{A} \succeq \mathbf{0}$ indicates that \mathbf{A} is a positive semi-definite matrix. The notation \mathbf{A}_{ij} refer to the $(i, j)^{\text{th}}$ element of matrix \mathbf{A} . The notations \mathbf{A}^H , \mathbf{A}^T , \mathbf{A}^* , and $\text{vec}(\mathbf{A})$ represent the conjugate transpose, transpose, conjugate, and vectorization of \mathbf{A} , respectively. The symbol \mathbf{A}^{-1} denotes the matrix inverse, while $\lambda_{\max}(\mathbf{A})$ denotes the maximum eigenvalue of \mathbf{A} . $\text{diag}(\mathbf{a})$ denotes a diagonal matrix with diagonal elements from vector \mathbf{a} . $\text{conj}(\mathbf{a})$ and $\text{arg}(\mathbf{a})$ represent the conjugate and phase of a complex vector \mathbf{a} , respectively. The symbol $\exp(\cdot)$ denotes the exponential function, while \odot and \otimes indicate the Hadamard and Kronecker products, respectively. The absolute value and Euclidean norm are denoted by $|\cdot|$ and $\|\cdot\|$, respectively. $\Re(\cdot)$ and $\Im(\cdot)$ represent the real and imaginary parts, respectively. The symbol $\mathbf{1}_M$ represents an all-one vector of length M , and \mathbf{I} is the identity matrix.

II. SYSTEM MODEL

As depicted in Fig. 1, an IRS-assisted ISAC system is studied, which consists of a BS featuring M radar antennas and N communication antennas, serving K single-antenna users. The transmission of statistically independent communication and radar signals is achieved through the utilization of a uniform linear array (ULA) at the BS, enabling the system to simultaneously detect targets and transmit data to K users. The IRS is composed of L reflecting elements, and $\Theta = \text{diag}(\phi_1, \phi_2, \dots, \phi_L)$ denotes the diagonal phase shift matrix, where $\phi_l = \exp(j\theta_l)$ represents the phase shift of the l -th reflecting element.

We assume that the targets are far away from the IRS, and the line of sight (LoS) link between the BS and the targets is much stronger than the link reflected from the IRS

to the targets due to the multiplicative path-loss law that characterizes the reflected power from the IRS. Therefore, only the LoS links between the BS and the targets are used to design the beam pattern. In addition, the IRS is deployed to enhance the communication signal and suppress the radar signal to improve the communication quality of the users. $\mathbf{H}_{dr} \in \mathbb{C}^{L \times N}$, $\mathbf{h}_{d,k} \in \mathbb{C}^{N \times 1}$, and $\mathbf{h}_{r,k} \in \mathbb{C}^{L \times 1}$ denote the mmWave channels between the IRS and the communication subsystem, between the k -th user and the communication subsystem, and between the k -th user and the IRS, respectively. $\mathbf{F}_{dr} \in \mathbb{C}^{L \times M}$, $\mathbf{f}_{d,k} \in \mathbb{C}^{M \times 1}$, and $\mathbf{f}_{r,k} \in \mathbb{C}^{L \times 1}$ denote the mmWave channels between the radar subsystem and the IRS, the k -th user and the radar subsystem, and the k -th user and the IRS, respectively.

We assume that all channels are known a priori in order to evaluate an upper bound of the system performance. In practice, the required channel state information can be obtained as detailed in [29]–[32]. Based on the mmWave channel model in [33], the channels can be expressed as

$$\begin{aligned} \mathbf{H}_{dr} &= \sum_{\ell=0}^{N_p} v^\ell \mathbf{a}_I^H(\theta_I^\ell, \phi_I^\ell) \mathbf{a}_B(\theta_B^\ell), \\ \mathbf{h}_{r,k} &= \sum_{\ell=0}^{N_p} v^\ell \mathbf{a}_{r,k}(\theta_{r,k}^\ell), \\ \mathbf{h}_{d,k} &= \sum_{\ell=0}^{N_p} v^\ell \mathbf{a}_B(\theta_{d,k}^\ell), \end{aligned} \quad (1)$$

where $v^\ell \in [0, N_p]$ represents the ℓ -th complex path gain, $\ell=0$ represents the LoS path. N_p is the number of non-line of sight paths. The azimuth and elevation angles of the IRS are denoted by θ^ℓ and ϕ^ℓ , respectively. $\mathbf{a}_B(\theta) = \frac{1}{\sqrt{N}} [\exp(-j \frac{2\pi d}{\lambda} \theta_i)]_{i \in I(N)} \in \mathbb{C}^{1 \times N}$ with $I(N) = \{n - (N-1)/2, \text{ for } n = 0, 1, \dots, N-1\}$ denotes the array response of the BS, where d is the spacing between adjacent antenna elements, and λ is the wavelength. $\mathbf{a}_I(\phi, \theta) = \mathbf{a}_I^{az}(\phi) \otimes \mathbf{a}_I^{el}(\theta) \in \mathbb{C}^{1 \times L}$ denotes the array response of the IRS, where $\mathbf{a}_I^{az}(\phi)$ and $\mathbf{a}_I^{el}(\theta)$ are defined as $\mathbf{a}_B(\theta)$. $\mathbf{a}_{r,k}(\theta_{r,k}) \in \mathbb{C}^{L \times 1}$ denotes the array response of the IRS, which is defined as $\mathbf{a}_B(\theta)$. $\theta_{r,k}$ and $\theta_{d,k}$ are the azimuth angles from the IRS to the k -th user and from BS to the k -th user.

Similarly, the radar channel between the radar subsystem and the IRS, the k -th user and the IRS, and the k -th user and the radar subsystem can be written as follows:

$$\begin{aligned} \mathbf{F}_{dr} &= \sum_{\ell=0}^{N_p} v^\ell \mathbf{a}_I^H(\theta_I^\ell, \phi_I^\ell) \mathbf{a}_R(\theta_R^\ell), \\ \mathbf{f}_{r,k} &= \sum_{\ell=0}^{N_p} v^\ell \mathbf{a}_{r,k}(\theta_{r,k}^\ell), \\ \mathbf{f}_{d,k} &= \sum_{\ell=0}^{N_p} v^\ell \mathbf{a}_R(\theta_{d,k}^\ell), \end{aligned} \quad (2)$$

where $\mathbf{a}_R(\theta) = \frac{1}{\sqrt{M}} [\exp(-j \frac{2\pi d}{\lambda} \theta_i)]_{i \in I(M)} \in \mathbb{C}^{1 \times M}$ with $I(M) = \{m - (M-1)/2, m = 0, 1, \dots, M-1\}$ denotes the array response of the radar subsystem.

By combing the direct link and the IRS-aided link, the signal

received at the k -th user can be formulated as

$$\begin{aligned} x_{k,j} &= \left(\mathbf{h}_{r,k}^H \Theta \mathbf{H}_{dr} + \mathbf{h}_{d,k}^H \right) \mathbf{w}_k d_{k,j} \\ &+ \left(\mathbf{h}_{r,k}^H \Theta \mathbf{H}_{dr} + \mathbf{h}_{d,k}^H \right) \sum_{i=1, i \neq k}^K \mathbf{w}_i d_{i,j} \\ &+ \left(\mathbf{f}_{r,k}^H \Theta \mathbf{F}_{dr} + \mathbf{f}_{d,k}^H \right) \mathbf{r}_{t,j} + n_{k,j}, \end{aligned} \quad (3)$$

where $\mathbf{w}_k \in \mathbb{C}^{N \times 1}$ is the beamforming vector, $d_{k,j}$ and $n_{k,j} \sim \mathcal{CN}(0, \sigma^2)$ are the transmitted symbol and the receiver noise at of the k -th user and time index j , respectively. Also, $\mathbf{r}_{t,j} \in \mathbb{C}^{M \times 1}$ is the j -th snapshot across the radar antennas [23]. The design of the radar beam pattern aims to optimize the transmit power in a given direction or to match a desired beam pattern. The beam pattern of a radar can be controlled by the RSC matrix \mathbf{R} , which is given by

$$\mathbf{R} = \frac{1}{J} \sum_{j=1}^J \mathbf{r}_{t,j} \mathbf{r}_{t,j}^H \quad (4)$$

where J being the the number of considered snapshots. Then, according to [23], the transmit beam pattern is defined as

$$P_t(\theta) = \mathbf{a}_R^H(\theta) \mathbf{R} \mathbf{a}_R(\theta) \quad (5)$$

To proceed, the signal to interference plus noise ratio (SINR) of the k -th user is given by

$$\begin{aligned} \gamma_k &= \frac{\left| \left(\mathbf{h}_{r,k}^H \Theta \mathbf{H}_{dr} + \mathbf{h}_{d,k}^H \right) \mathbf{w}_k \right|^2}{\sum_{i=1, i \neq k}^K \left| \left(\mathbf{h}_{r,k}^H \Theta \mathbf{H}_{dr} + \mathbf{h}_{d,k}^H \right) \mathbf{w}_i \right|^2 + \left| \left(\mathbf{f}_{r,k}^H \Theta \mathbf{F}_{dr} + \mathbf{f}_{d,k}^H \right) \mathbf{r}_t \right|^2 + \sigma^2} \\ &= \frac{\left| \tilde{\mathbf{h}}_k \mathbf{w}_k \right|^2}{\sum_{i=1, i \neq k}^K \left| \tilde{\mathbf{h}}_k \mathbf{w}_i \right|^2 + \left| \tilde{\mathbf{f}}_k \mathbf{r}_t \right|^2 + \sigma^2}, \end{aligned} \quad (6)$$

where $\tilde{\mathbf{h}}_k = \mathbf{h}_{r,k}^H \Theta \mathbf{H}_{dr} + \mathbf{h}_{d,k}^H$ and $\tilde{\mathbf{f}}_k = \mathbf{f}_{r,k}^H \Theta \mathbf{F}_{dr} + \mathbf{f}_{d,k}^H$.

A. Problem Formulation

In this paper, we consider a separated antenna layout to achieve sensing and communication simultaneously, and two independent but related optimization problems are formulated. An ideal radar beam pattern can be obtained before designing the IRS phase shifts and the beamforming of the communication subsystem. Firstly, the optimization of the beam pattern can be formulated as a constrained least-squares problem as

$$\min_{\beta, \mathbf{R}} \sum_{c=1}^C \left| \beta P(\theta_c) - \mathbf{a}_R^H(\theta_c) \mathbf{R} \mathbf{a}_R(\theta_c) \right|^2 \quad (7a)$$

$$\text{s.t. } \beta > 0, \quad (7b)$$

$$\text{diag}(\mathbf{R}) = \frac{P_r}{M} \mathbf{I}, \quad (7c)$$

$$\mathbf{R} \succeq \mathbf{0}, \mathbf{R} = \mathbf{R}^H, \quad (7d)$$

where β denotes a scaling factor, $\{\theta_c\}_{c=1}^C$ denotes the angles of interest, typically from -90° to 90° , C is the number of angles considered, and $P(\theta_c)$ represents the desired beam pattern of the MIMO radar, P_r is the power budget of the radar subsystem. The constraint (7c) ensures that all the radar antennas emit the same power level. In the following, we

proceed to design the communication beamforming and IRS design to enhance the transmission rate and suppress the interference from the radar system to the users. Given the RSC matrix \mathbf{R} , we formulate the optimization problem of the sum transmission rate as

$$\max_{\mathbf{w}_k, \Theta} \sum_{k=1}^K \log(1 + \gamma_k) \quad (8a)$$

$$s.t. \sum_{k=1}^K \mathbf{w}_k^H \mathbf{w}_k \leq P_c, \quad (8b)$$

$$|\phi_l| = 1, l \in L, \quad (8c)$$

where P_c represents the transmit power budget at the communication subsystem and (8b) accounts for the maximum transmit power limit of the communication system.

Proposition 1: Equation (8a) can be reformulated as

$$\max_{\mathbf{w}_k, \Theta, \mathbf{p}} f_1 = \frac{1}{\ln 2} \sum_{k=1}^K \left(\ln(1 + p_k) - p_k + \frac{(1 + p_k)\gamma_k}{1 + \gamma_k} \right), \quad (9)$$

where $\mathbf{p} = [p_1, \dots, p_K]$ denotes an auxiliary vector introduced through the Lagrangian dual transformation [34].

Proof: See Appendix A.

By taking the partial derivative of (9) with respect to p_k and setting it to zero, we can obtain the optimal value of the k -th auxiliary variable as $\hat{p}_k = \gamma_k$. Subsequently, the joint optimization of \mathbf{w}_k and Θ in (9) can be simplified with the given value of \mathbf{p} as

$$\max_{\mathbf{w}_k, \Theta} f_2 = \sum_{k=1}^K \frac{(1 + p_k)\gamma_k}{1 + \gamma_k} \quad (10)$$

s.t. (8b), (8c),

Define $\bar{p}_k \triangleq 1 + p_k$ and substitute γ_k in (6) into (10), we can reformulate (10) as

$$\max_{\mathbf{w}_k, \Theta} f_2 = \sum_{k=1}^K \frac{\bar{p}_k |\tilde{\mathbf{h}}_k \mathbf{w}_k|^2}{\sum_{i=1}^K |\tilde{\mathbf{h}}_i \mathbf{w}_i|^2 + |\tilde{\mathbf{f}}_k \mathbf{r}_t|^2 + \sigma^2} \quad (11)$$

s.t. (8b), (8c).

Consequently, the logarithmic function in (8a) can be easily addressed or simplified.

III. ACHIEVABLE SUM RATE MAXIMIZATION

In this section, we provide a closed-form solution for the RSC matrix \mathbf{R} , the communication beamforming vector \mathbf{w}_k , and the IRS matrix Θ . Firstly, we formulate the radar beampattern design as a least-squares problem, which has a feasible closed-form solution through a series of mathematical derivations. Subsequently, we leverage the QT variation and employ the AO algorithm to obtain efficient solutions for both the beamforming vector and the IRS phase shifts at each iteration.

A. Designing the Covariance Matrix for Radar Signals

The radar beampattern, crucial for radar detection, is determined by the RSC matrix \mathbf{R} , and the optimization of the RSC matrix \mathbf{R} can be cast as a constrained least-squares problem as

$$\min_{\beta, \mathbf{R}} \sum_{c=1}^C |\beta P(\theta_c) - \mathbf{a}_R^H(\theta_c) \mathbf{R} \mathbf{a}_R(\theta_c)|^2 \quad (12)$$

s.t. (7b), (7c), (7d).

Inspired by the pseudo covariance matrix synthesis algorithm proposed in [35], we utilize a scheme that effectively reduces the complexity associated with the RSC matrix. To achieve this, we vectorize the objective function, facilitating the design of efficient optimization procedures as

$$f(\mathbf{R}, \beta) = \sum_{c=1}^C \left| \beta P(\theta_c) - \text{vec}(\mathbf{V}(\theta_c))^H \mathbf{r}_v \right|^2, \quad (13)$$

where $\mathbf{V}(\theta_c) = \mathbf{a}_R(\theta_c) \mathbf{a}_R^H(\theta_c)$ and $\mathbf{r}_v = \text{vec}(\mathbf{R})$.

Define $\mathbf{v}_1 \triangleq [\Re(\mathbf{v}_d^T) \ \Im(\mathbf{v}_d^T)]^T$ and $\mathbf{r}_1 \triangleq [\Re(\mathbf{r}_d^T) \ \Im(\mathbf{r}_d^T)]^T$, where $\mathbf{v}_d = [\mathbf{V}_{12}, \dots, \mathbf{V}_{1M}, \mathbf{V}_{23}, \dots, \mathbf{V}_{(M-1)M}]^T$, and $\mathbf{r}_d = [\mathbf{R}_{12}, \dots, \mathbf{R}_{1M}, \mathbf{R}_{23}, \dots, \mathbf{R}_{(M-1)M}]^T$.

Also, let us introduce $\mathbf{v}_2 = [\mathbf{V}_{11}, \dots, \mathbf{V}_{MM}]^T = \mathbf{1}_M$, and $\mathbf{r}_2 = [\mathbf{R}_{11}, \dots, \mathbf{R}_{MM}]^T = \frac{P_r}{M} \mathbf{1}_M$.

Thus, we can transform (13) to

$$\begin{aligned} f(\mathbf{r}_x) &= \sum_{c=1}^C \left([2\mathbf{v}_1^T \ \mathbf{v}_2^T] \begin{bmatrix} \mathbf{r}_1 \\ \mathbf{r}_2 \end{bmatrix} - \beta P(\theta_c) \right)^2 \\ &= 4 \sum_{c=1}^C \left([\mathbf{v}_1^T, -\frac{1}{2}P(\theta_c)] \begin{bmatrix} \mathbf{r}_1 \\ \beta \end{bmatrix} + \frac{1}{2}P_r \right)^2 \quad (14) \\ &= 4 \sum_{c=1}^C (\mathbf{v}_x^T(\theta_c) \mathbf{r}_x + \frac{1}{2}P_r)^2, \end{aligned}$$

where $\mathbf{v}_x^T(\theta_c) = [\mathbf{v}_1^T, -\frac{1}{2}P(\theta_c)]$ and $\mathbf{r}_x = [\mathbf{r}_1 \ \beta]^T$. Computing the derivative with respect to \mathbf{r}_x in (14) and making it zero, the optimal closed-form solution can be derived as

$$\mathbf{r}_x = -\frac{P_r}{2} \mathbf{V}_x^{-1} \mathbf{v}_u, \quad (15)$$

where $\mathbf{V}_x = \sum_{c=1}^C \mathbf{v}_x(\theta_c) \mathbf{v}_x^H(\theta_c)$ and $\mathbf{v}_u = \sum_{c=1}^C \mathbf{v}_x(\theta_c)$. The RSC matrix \mathbf{R}_{rad} can be constructed by rearranging \mathbf{r}_x , and setting the last entry of \mathbf{r}_x equal to β . However, there is no guarantee that \mathbf{R}_{rad} is a positive semidefinite matrix. Then, we apply the eigenvalue decomposition to ensure $\mathbf{R}_{rad} \succeq \mathbf{0}$, and the specific RSC matrix is reconstructed by

$$\mathbf{R}_{rad} = \mathbf{U} \text{diag}(\tilde{\sigma}) \mathbf{U}^H, \quad (16)$$

where $\tilde{\sigma}$ is a vector, which is employed as a substitution for the negative eigenvalues observed in the original matrix. Specifically, the negative eigenvalues are replaced by their absolute values or zeros in order to ensure the integrity and validity of the resulting vector, and $\mathbf{U} = [\mathbf{u}_1, \dots, \mathbf{u}_{N_r}]$ represents the corresponding eigenvectors [35].

To proceed, the diagonal normalization method is implemented to normalize the diagonal elements of the matrix to ensure the constraint (7c) as

$$\mathbf{R} = \mathbf{T} \mathbf{R}_{rad} \mathbf{T}^H, \quad (17)$$

where \mathbf{T} is constructed as a diagonal matrix, where its diagonal elements are identical to the diagonal elements of $\sqrt{\frac{P_r}{M}} \mathbf{R}_{rad}$.

B. Communication Beamforming Design

After obtaining the specific RSC matrix \mathbf{R} from (17), we can reformulate problem (10) as

$$\max_{\mathbf{w}_k, \Theta} f_3 = \sum_{k=1}^K \frac{\bar{p}_k |\tilde{\mathbf{h}}_k \mathbf{w}_k|^2}{\sum_{i=1}^K |\tilde{\mathbf{h}}_i \mathbf{w}_i|^2 + |\tilde{\mathbf{f}}_k \mathbf{r}_t|^2 + \sigma^2} \quad (18a)$$

$$s.t. \text{ (8b)}. \quad (18b)$$

Problem (18) is a multi-ratio fractional programming problem, and the optimization variables \mathbf{w}_k and Θ are mutually coupled. To address this, we adopt the AO algorithm and the QT technique [34] to reframe problem (18) into a biconvex problem of the following form

$$\max_{\mathbf{w}_k, \Theta} f_4 = \sum_{k=1}^K 2\sqrt{\bar{p}_k} \Re\{s_k^* \tilde{\mathbf{h}}_k \mathbf{w}_k\} - |s_k|^2 \left(\sum_{i=1}^K |\tilde{\mathbf{h}}_i \mathbf{w}_i|^2 + |\tilde{\mathbf{f}}_k \mathbf{r}_t|^2 + \sigma^2 \right) \quad (19)$$

$$s.t. \text{ (8b)},$$

where $\mathbf{s} = [s_1, \dots, s_K]^T$ denotes a set of auxiliary vector introduced by the QT technique. The optimal value of s_k can be obtained by setting the partial derivative of f_4 with respect to s_k to zero as

$$s_k^{opt} = \frac{\sqrt{\bar{p}_k} \tilde{\mathbf{h}}_k \mathbf{w}_k}{\sum_{i=1}^K |\tilde{\mathbf{h}}_i \mathbf{w}_i|^2 + |\tilde{\mathbf{f}}_k \mathbf{r}_t|^2 + \sigma^2}. \quad (20)$$

Thus, by applying the Lagrangian multiplier method, the optimal value of \mathbf{w}_k can be derived as

$$\mathbf{w}_k^{opt} = \sqrt{\bar{p}_k} s_k \left(\mu \mathbf{I} + |s_k|^2 \sum_{i=1}^K \tilde{\mathbf{h}}_i^H \tilde{\mathbf{h}}_i \right)^{-1} \tilde{\mathbf{h}}_k^H, \quad (21)$$

where μ is the Lagrange multiplier associated with the power constraint in (8b), which can be computed by using the bisection search method based on the following lemma.

Lemma 1: μ in (21) is determined by

$$\hat{\mu} = \left\{ \mu \geq 0 \mid \sum_{k=1}^K \mathbf{w}_k^H \mathbf{w}_k = P_{\max} \right\}. \quad (22)$$

Proof: See Appendix B.

C. Optimization for the IRS Phase Shifts

In this section, we the IRS phase shifts for the k -th user, given the optimal \mathbf{w}_k^{opt} . Specifically, $\tilde{\mathbf{h}}_k$ and $\tilde{\mathbf{f}}_k$ can be expressed as

$$\begin{aligned} \tilde{\mathbf{h}}_k &= \mathbf{h}_{r,k}^H \Theta \mathbf{H}_{dr} + \mathbf{h}_{d,k}^H = \tilde{\boldsymbol{\theta}} \text{diag}(\mathbf{h}_{r,k}^H) \mathbf{H}_{dr} + \mathbf{h}_{d,k}^H \\ &= [\tilde{\boldsymbol{\theta}} \quad \mathbf{1}] \begin{bmatrix} \text{diag}(\mathbf{h}_{r,k}^H) \mathbf{H}_{dr} \\ \mathbf{h}_{d,k}^H \end{bmatrix} = \boldsymbol{\theta} \mathbf{A}_k \end{aligned} \quad (23)$$

$$\begin{aligned} \tilde{\mathbf{f}}_k &= \mathbf{f}_{r,k}^H \Theta \mathbf{F}_{dr} + \mathbf{f}_{d,k}^H = \tilde{\boldsymbol{\theta}} \text{diag}(\mathbf{f}_{r,k}^H) \mathbf{F}_{dr} + \mathbf{f}_{d,k}^H \\ &= [\tilde{\boldsymbol{\theta}} \quad \mathbf{1}] \begin{bmatrix} \text{diag}(\mathbf{f}_{r,k}^H) \mathbf{F}_{dr} \\ \mathbf{f}_{d,k}^H \end{bmatrix} = \boldsymbol{\theta} \mathbf{B}_k \end{aligned} \quad (24)$$

where $\boldsymbol{\theta} = [\tilde{\boldsymbol{\theta}} \quad \mathbf{1}]$ with $\tilde{\boldsymbol{\theta}} = [\exp(j\phi_1), \dots, \exp(j\phi_L)]$. Then, problem (18) can be reformulated as

$$\max_{\boldsymbol{\theta}} f_5(\boldsymbol{\theta}) = \sum_{k=1}^K \frac{\bar{p}_k |\boldsymbol{\theta} \mathbf{A}_k \mathbf{w}_k|^2}{\sum_{i=1}^K |\boldsymbol{\theta} \mathbf{A}_i \mathbf{w}_i|^2 + |\boldsymbol{\theta} \mathbf{B}_k \mathbf{r}_t|^2 + \sigma^2}. \quad (25)$$

Similarly, we define $\mathbf{c}_k \triangleq \mathbf{A}_k \mathbf{w}_k$ and apply the QT technique to (25) and hence obtain

$$\max_{\boldsymbol{\theta}} f_6(\boldsymbol{\theta}, \mathbf{b}) = \sum_{k=1}^K 2\sqrt{\bar{p}_k} \Re\{b_k^* \boldsymbol{\theta} \mathbf{c}_k\} - |b_k|^2 \left\{ \sum_{i=1}^K |\boldsymbol{\theta} \mathbf{c}_i|^2 + |\boldsymbol{\theta} \mathbf{B}_k \mathbf{r}_t|^2 + \sigma^2 \right\}, \quad (26)$$

where $\mathbf{b} = [b_1, \dots, b_K]$ represents an auxiliary vector introduced by the QT technique. The Lagrange multiplier method is used to determine the optimal value of b_k as

$$b_k^{opt} = \frac{\sqrt{\bar{p}_k} \boldsymbol{\theta} \mathbf{c}_k}{\sum_{i=1}^K |\boldsymbol{\theta} \mathbf{c}_i|^2 + |\boldsymbol{\theta} \mathbf{B}_k \mathbf{r}_t|^2 + \sigma^2}. \quad (27)$$

Hence, given a specific value of b_k , we proceed to simplifying (26) as

$$\max_{\boldsymbol{\theta}} f_7(\boldsymbol{\theta}) = -\boldsymbol{\theta} \mathbf{E} \boldsymbol{\theta}^H + 2\Re\{\boldsymbol{\theta} \mathbf{g}\} - d_1, \quad (28)$$

where $\mathbf{E} = \sum_{k=1}^K |b_k|^2 \sum_{i=1}^K \mathbf{c}_i \mathbf{c}_i^H + \mathbf{B}_k \mathbf{R} \mathbf{B}_k^H$, $\mathbf{g} = \sum_{k=1}^K \sqrt{\bar{p}_k} b_k^* \mathbf{c}_k$

and $d_1 = \sum_{k=1}^K |b_k|^2 \sigma^2$. Problem (28) is a quadratically constrained quadratic programming problem and its objective becomes

$$\min_{\boldsymbol{\theta}} f_7(\boldsymbol{\theta}) = \boldsymbol{\theta} \mathbf{E} \boldsymbol{\theta}^H - 2\Re\{\boldsymbol{\theta} \mathbf{g}\}. \quad (29)$$

In the following, we employ the MM and CCM methods to solve problem (29), respectively.

1) MM method: To address the problem (29), we utilize the MM algorithm, which involves solving a series of solvable subproblems. This approach allows us to iteratively approximate the objective function [36].

Proposition 2: $\boldsymbol{\theta}^{(m)}$ is defined as the vector at the m -th iteration, thus the objective function (29) at the m -th iteration for any given $\boldsymbol{\theta}^{(m)}$ can be approximated as

$$\begin{aligned} f_7(\boldsymbol{\theta}) &\leq \boldsymbol{\theta} \mathbf{P} \boldsymbol{\theta}^H - 2\Re\left\{ \boldsymbol{\theta} \left((\mathbf{P} - \mathbf{E}) \tilde{\boldsymbol{\theta}}^H + \mathbf{g} \right) \right\} + \tilde{\boldsymbol{\theta}} (\mathbf{P} - \mathbf{E}) \tilde{\boldsymbol{\theta}}^H \\ &= \lambda_{\max}(\mathbf{E}) \|\boldsymbol{\theta}\|^2 - 2\Re\left\{ \boldsymbol{\theta} \left((\lambda_{\max}(\mathbf{E}) \mathbf{I} - \mathbf{E}) \tilde{\boldsymbol{\theta}}^H + \mathbf{g} \right) \right\} \\ &\quad + \tilde{d} = g(\boldsymbol{\theta} | \boldsymbol{\theta}^{(m)}) \end{aligned} \quad (30)$$

where $\tilde{\boldsymbol{\theta}}$ represents an approximate solution to $\boldsymbol{\theta}$ obtained in the previous iteration, \tilde{d} and \mathbf{P} are defined as $\tilde{d} \triangleq \tilde{\boldsymbol{\theta}} (\lambda_{\max}(\mathbf{E}) \mathbf{I} - \mathbf{E}) \tilde{\boldsymbol{\theta}}^H$ and $\mathbf{P} \triangleq \lambda_{\max}(\mathbf{E}) \mathbf{I}$, respectively. By adopting a surrogate function for the objective function in

(29), the original problem (29) is transformed into a modified problem as

$$\min_{\boldsymbol{\theta}} \lambda_{\max}(\mathbf{E}) \|\boldsymbol{\theta}\|^2 - 2\Re\{\boldsymbol{\theta}\bar{\mathbf{g}}\}, \quad (31)$$

where $\bar{\mathbf{g}} = (\lambda_{\max}(\mathbf{E})\mathbf{I} - \mathbf{E})\tilde{\boldsymbol{\theta}}^H + \mathbf{g}$. It can be easily shown that $\|\boldsymbol{\theta}\|^2 = L + 1$ since $|\boldsymbol{\theta}(l)| = 1$ in the IRS. The term $\Re\{\boldsymbol{\theta}\bar{\mathbf{g}}\}$ can be maximized when the two vectors $\boldsymbol{\theta}$ and $\bar{\mathbf{g}}$ are identical. Thus, given $\mathbf{c} = [c_1, \dots, c_N] = (\lambda_{\max}(\mathbf{E})\mathbf{I} - \mathbf{E})\tilde{\boldsymbol{\theta}}^H + \mathbf{g}$, the optimal solution to (31) is derived as

$$\boldsymbol{\theta}^{opt} = [\exp(j \arg(c_1)), \dots, \exp(j \arg(c_{L+1}))]. \quad (32)$$

We summarize the MM algorithm as *Algorithm 1*.

Algorithm 1 MM Algorithm

Initialization: A feasible solution $\boldsymbol{\theta}^{(0)}$ and $m = 0$.

repeat

Obtain $\bar{\mathbf{g}}^{(m)} = (\lambda_{\max}(\mathbf{E})\mathbf{I} - \mathbf{E})(\boldsymbol{\theta}^{(m)})^H + \mathbf{g}$.

Obtain the optimal phase shifts $\boldsymbol{\theta}^{opt(m)}$ in the m iteration according to (32).

Update $\boldsymbol{\theta}^{(m+1)} = \boldsymbol{\theta}^{opt(m)}$ and calculate $f_7(\boldsymbol{\theta}^{(m+1)})$.

Set $m \leftarrow m + 1$.

until convergence

2) *CCM method:* We provide another method called the CCM algorithm to obtain the optimal phase shifts of the k -th user. The principal idea is to derive a gradient descent algorithm on the manifold space [37]. Accordingly, problem (29) can be reformulated as

$$\min_{\boldsymbol{\theta}} f_9(\boldsymbol{\theta}) = \boldsymbol{\theta}(\mathbf{E} + \kappa\mathbf{I})\boldsymbol{\theta}^H - 2\Re\{\boldsymbol{\theta}\mathbf{g}\}, \quad (33)$$

where κ is a constant that controls the convergence of the algorithm. Since $\kappa\boldsymbol{\theta}\boldsymbol{\theta}^H = \kappa(L + 1)$, problem (33) is equivalent to problem (29). We define the feasible set of problem (33) as \mathcal{S}^{L+1} , which is given by $L + 1$ complex circles, and each complex circle can be represented as $\mathcal{S} \triangleq \{z \in \mathbb{C} | \Re\{z\}^2 + \Im\{z\}^2 = 1\}$. The set \mathcal{S} can be regarded as a sub-manifold embedded in the complex space \mathbb{C} , and the product of $L + 1$ circles corresponds to a sub-manifold of \mathbb{C}^{L+1} [37]. Hence, the manifold of (33) can be given as $\mathcal{S}^{L+1} \triangleq \{\mathbf{z} \in \mathbb{C}^{L+1} | |\mathbf{z}_l| = 1, \text{ for } l \in [1, L + 1]\}$, where \mathbf{z}_l is the l -th element of a vector \mathbf{z} . Next, we detail the steps of the CCM algorithm for solving problem (33) iteratively.

1) The search direction: We first define the objective function of problem (33) at the i -th iteration as $f_9(\boldsymbol{\theta}^{(i)})$. Subsequently, the search direction for problem (33) is determined to be opposite to the gradient in the Euclidean space of $f_9(\boldsymbol{\theta}^{(i)})$ as

$$\mathbf{z}^{(i)} = -\nabla_{\boldsymbol{\theta}} f_9(\boldsymbol{\theta}^{(i)}) = -2(\mathbf{E} + \kappa\mathbf{I})(\boldsymbol{\theta}^{(i)})^H + 2\mathbf{g}. \quad (34)$$

2) Projection search direction on the tangent space: The optimization step on the manifold space finds the Riemannian gradient of f_9 at the point $\boldsymbol{\theta}^{(i)}$ in the current tangent space $\mathcal{T}_{\boldsymbol{\theta}^{(i)}}\mathcal{S}^{L+1}$ [38]. The search direction $\mathbf{z}^{(i)}$ in the Euclidean space is projected onto $\mathcal{T}_{\boldsymbol{\theta}^{(i)}}\mathcal{S}^{L+1}$ and the Riemannian gradient at $\boldsymbol{\theta}^{(i)}$ of $f_9(\boldsymbol{\theta}^{(i)})$ is given as

$$\mathbf{P}_{\mathcal{X}}(\mathbf{z}^{(i)}) = \mathbf{z}^{(i)} - \Re\{\text{conj}(\mathbf{z}^{(i)}) \odot \boldsymbol{\theta}^{(i)}\} \odot \boldsymbol{\theta}^{(i)}, \quad (35)$$

where $X = \mathcal{T}_{\boldsymbol{\theta}^{(i)}}\mathcal{S}^{L+1}$.

3) Updated descent on the tangent space: $\boldsymbol{\theta}^{(i)}$ on the tangent space $\mathcal{T}_{\boldsymbol{\theta}^{(i)}}\mathcal{S}^{L+1}$ can be performed as

$$\hat{\boldsymbol{\theta}}^{(i)} = \boldsymbol{\theta}^{(i)} + \zeta \mathbf{P}_{\mathcal{X}}(\mathbf{z}^{(i)}), \quad (36)$$

where ζ is the step size.

4) Retraction operation: As $\hat{\boldsymbol{\theta}}^{(i)}$ is not in \mathcal{S}^{L+1} , $\hat{\boldsymbol{\theta}}^{(i)}$ is mapped to the manifold \mathcal{S}^{L+1} by a retraction operation, and we normalize each element of $\hat{\boldsymbol{\theta}}^{(i)}$ to unity as

$$\boldsymbol{\theta}^{(i+1)} = \hat{\boldsymbol{\theta}}^{(i)} \odot \frac{1}{\hat{\boldsymbol{\theta}}^{(i)}}. \quad (37)$$

The following theorem is utilized to establish the range of parameters κ and ζ that guarantee the convergence of the CCM algorithm.

Theorem 1 [37]: Let us denote by $\lambda_{\mathbf{E}}$ and $\lambda_{\mathbf{E} + \kappa\mathbf{I}}$ the maximum eigenvalue of matrices \mathbf{E} and $\mathbf{E} + \kappa\mathbf{I}$, respectively. If κ and ζ satisfy the following conditions,

$$\kappa \geq \frac{L + 1}{8} \lambda_{\mathbf{E}} + \|\mathbf{g}\|_2, \quad 0 < \zeta < 1/\lambda_{(\mathbf{E} + \kappa\mathbf{I})}, \quad (38)$$

the CCM algorithm generates a non-increasing sequence until convergence.

We summarize CCM algorithm as *Algorithm 2*.

Algorithm 2 CCM Algorithm

Initialization: $i = 0$, and a feasible solution $\boldsymbol{\theta}^{(0)}$.

repeat

Obtain the search direction $\mathbf{z}^{(i)}$ in (34).

Obtain the tangent space projection of $\mathbf{z}^{(i)}$ from (35).

Update $\hat{\boldsymbol{\theta}}^{(i)}$ on the tangent space by (36).

Update $\boldsymbol{\theta}^{(i+1)}$ to the manifold \mathcal{S}^{L+1} by (37).

Update $i \leftarrow i + 1$.

until convergence

D. Complexity Analysis

In the design of the RSC matrix, the calculation of (15) incurs the highest computational cost, where \mathbf{V}_x is a square matrix of size $M^2 - M + 1$. The eigen-decomposition can be applied to approximate the inverse of \mathbf{V}_x and then the computational complexity of (15) is $\mathcal{O}(\Gamma(M^2 - M + 1)^2)$, where Γ denotes the rank of \mathbf{V}_x . The complexity order of the ED in (16) and the DN in (17) is $\mathcal{O}(M^3)$ and $4M^2$ flops. Next, we analyze the complexity of the AO algorithm and denote the number of iterations by I_{AO} . For the communication beamforming vector, there are three closed-form expressions in (20), (21), and (22), for which the complexity order is $\mathcal{O}_2 = K(\mathcal{O}(N^3) + \mathcal{O}(KN^2) + \mathcal{O}(N^2))$. For the IRS design, the complexity of the algorithm using the MM is $\mathcal{O}_3 = K((L + 1)^3 + I_m(L + 1)^2)$ and the CCM algorithm requires $\mathcal{O}_4 = K((L + 1)^3 + I_c(L + 1)^2)$, where I_m and I_c are the corresponding numbers of iterations. In summary, the overall complexity of the MM algorithm is $\mathcal{O}(\mathcal{O}_1 + I_{AO}\mathcal{O}_2\mathcal{O}_3)$, while that of the CCM algorithm is $\mathcal{O}(\mathcal{O}_1 + I_{AO}\mathcal{O}_2\mathcal{O}_4)$.

IV. PERFORMANCE EVALUATION

In this section, numerical simulations are provided to analyze the performance of the considered IRS-assisted ISAC

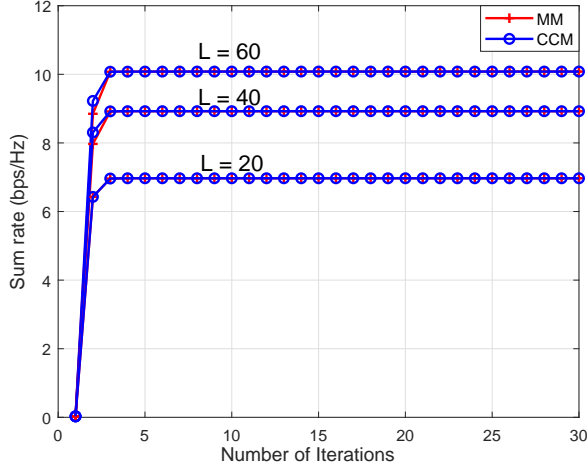


Fig. 2. Convergence of the proposed algorithm.

system. In the system, the BS is equipped with $M = 4$ radar antennas and $N = 4$ communication antennas. Also, we consider four single-antenna users ($K = 4$), and an IRS equipped with $L = 20$ reflecting elements. The noise power is set to $\sigma^2 = -80$ dBm. Moreover, we consider the presence of three targets positioned at the angles -30° , 0° , and 30° relative to the BS, and consider a mesh grid with a 1° interval ranging from -90° to 90° . The following benchmark schemes are considered for comparison with the proposed algorithm:

- 1) *Discrete phase shifts*: One bit quantized values for the phase shifts of the IRS are applied.
- 2) *Random phase shifts*: The beamforming vector and the radar RSC matrix are optimized, while the phase shifts of the IRS are randomly generated.
- 3) *Without IRS*: The system includes the direct transmission between the ISAC BS and the user without the IRS, and the RSC matrix and the communication beamforming are optimized.

Firstly, we demonstrate the convergence property of the proposed algorithm in Fig. 2. The MM and CCM algorithms show different upward trends before convergence and reach nearly identical convergence performance. These results verify the derivation in Section III-C.

Next, we characterize the impact of the transmit power for communication P_c on the sum rate in Fig. 3. The performance of the system is effectively improved as the power increases. The optimized IRS shows the best performance, while the IRS with discrete phase shifts incurs some performance loss because of the quantization error. Additionally, the proposed scheme is superior to the case of IRS with random phase shifts, which validates the benefits of optimizing the phase shifts. Finally, the schemes with the IRS show a significant increase in the sum rate compared to the case without the IRS.

Fig. 4 depicts the influence of the number of IRS reflecting elements L on the sum rate. The sum rate increases with the increment in the number of IRS reflecting elements in all considered schemes. This phenomenon is attributed to the joint optimization of the BS beamforming and IRS phase

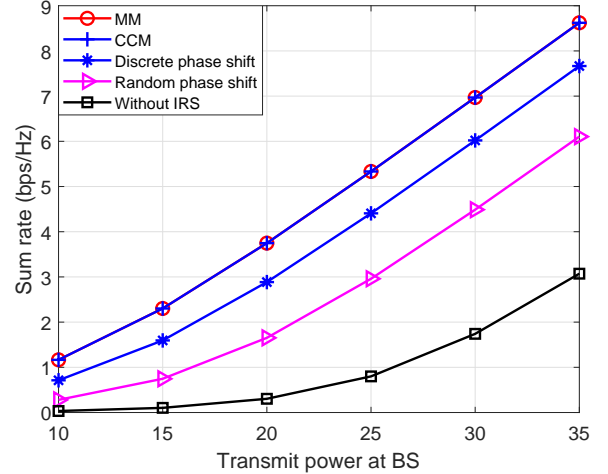


Fig. 3. Sum rate with respect to P_c .

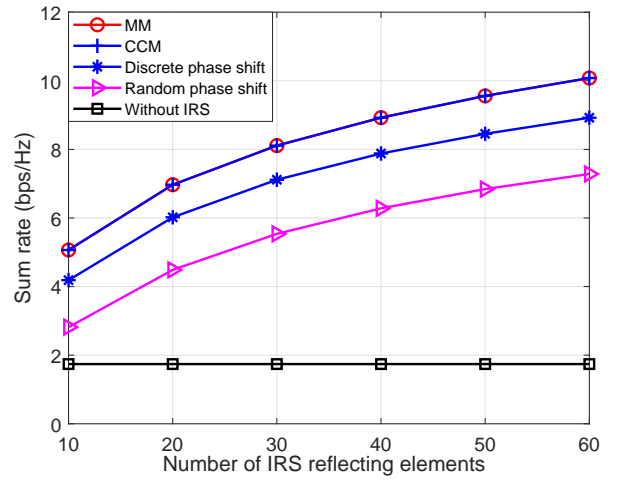
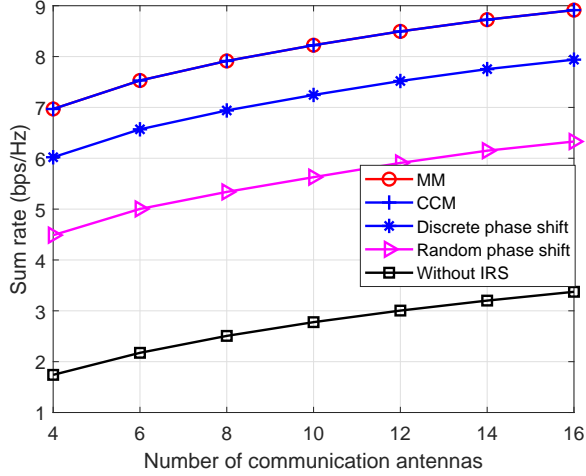
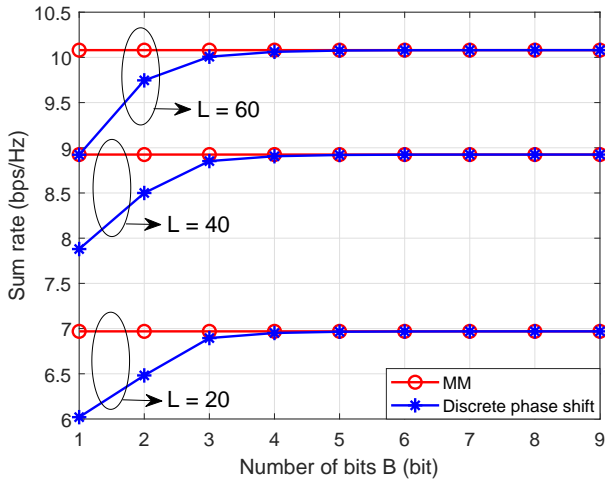


Fig. 4. Sum rate with respect to L .

shifts matrix. As the number of IRS reflecting elements increases, the sum rate obtained with the IRS experiences a substantial enhancement compared to the scheme without the IRS. This enhancement is attributed to the introduction of stronger reflected signals resulting from the increased L , thereby enhancing the received power.

In Fig. 5, we illustrate the sum rate as a function of the number of transmit antennas for communication. The utilization of multi-antenna techniques has been extensively validated to enhance the communication performance. By employing appropriate beamforming strategies, it is evident that the communication performance is markedly enhanced in all schemes as the number of communication antennas increases from 4 to 16. However, comparing the results with those shown in Fig. 4, it appears to be more cost-effective to increase the number of reflective elements of the IRS to achieve similar gains.

In Fig. 6, we examine the influence of the discrete phase resolution of the IRS on the sum rate and assess the disparity between continuous and discrete phase shifts utilizing the MM

Fig. 5. Sum rate with respect to N .Fig. 6. Sum rate with respect to B .

and CCM algorithms. The setting with continuous phases represents an upper limit of the discrete phase counterpart, and the discrepancy between them diminishes progressively as B increases. The numerical results show that $B = 3$ bits are adequate to attain optimal performance.

In this paper, we use the detection probability to measure the sensing performance according to [39], where P_{FA} denotes the false alarm probability of the radar system, i.e., the probability that the system still determines the presence of a target object when only noise is present. Fig. 7 shows that the overall detection probability increases with increasing the radar SNR, and, at the same SNR, the detection probability decreases with decreasing the radar false alarm probability, and, as the false alarm probability decreases, the detection probability shifts to the right. The rationale is that a higher false alarm probability characterizes a higher error tolerance of the system, leading to an increased detection probability.

In Fig. 8, we evaluate the relationship between the radar transmit power and the detection probability when $P_{FA} = 10^{-5}$. We see that curves of the detection probability shift

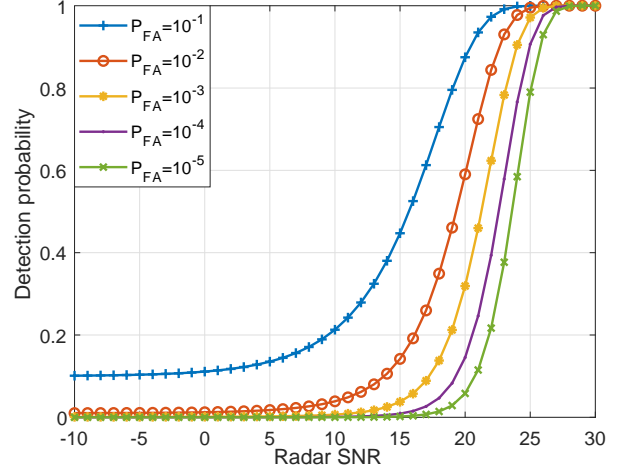


Fig. 7. Radar detection probability with respect to the radar SNR.

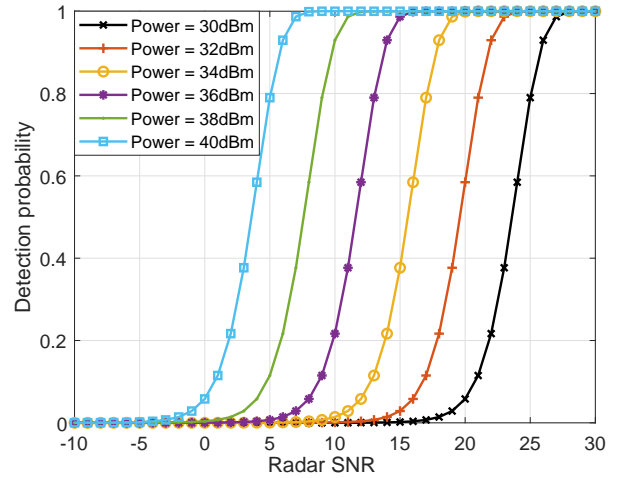


Fig. 8. Radar detection probability with respect to the radar SNR.

to the left when increasing the power. This is because, as the radar transmit power increases, the radar beampattern has a higher beampattern gain, which can significantly improve the quality of the radar SNR and increase the probability of detection for low values of the SNR.

Finally, the relationship between the designed beampattern (Designed BP) and the desired BP (Desired BP) under different antenna configurations is illustrated in Fig. 9 to evaluate the algorithm developed in Sec. III-A. It can be observed that the designed BP can better match the desired one by increasing the number of antennas. However, the scheme with a small number of antennas can basically satisfy the constraints imposed and does not cause much interference to the communication system.

V. CONCLUSION

This paper investigated the application of IRS in an ISAC system operating in the mmWave band. The main objectives were to maximize the sum rate and minimize the beampattern error. Closed-form expressions were derived for the radar

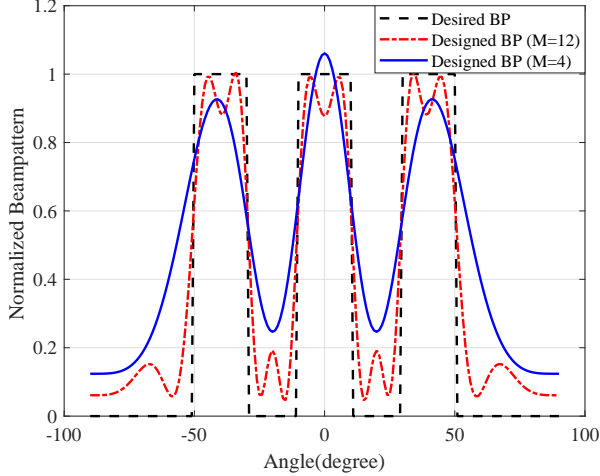


Fig. 9. Radar beam patterns.

RSC matrix, the communication beamforming vector, and the IRS phase shifts. The proposed scheme utilized the MM and CCM algorithms to optimize the IRS phase shifts, effectively reducing the computational complexity. Through numerical simulations, the performance of the proposed algorithm was validated, demonstrating that the utilization of the IRS can significantly enhance the transmission rate of an ISAC system.

APPENDIX

A. Proof to Proposition 1

The equation (9) can be considered as a concave function that is differentiable with respect to p_k when given a fixed value of λ_k . Taking the derivative of (9) about p_k and equating it to zero

$$\frac{\partial f_1}{\partial p_k} = \frac{1}{\ln 2} \sum_{k=1}^K \left(\frac{1}{1+p_k} - 1 + \frac{\gamma_k}{1+\gamma_k} \right) = 0. \quad (39)$$

Then, we obtain $\hat{p}_k = \gamma_k$. Taking p_k back to (9) yields (8a). Therefore, the two problems share equivalent optimal objective values, guaranteeing their equivalence.

B. Proof to Lemma 1

(21) can be re-arranged as Equation

$$\hat{\mathbf{W}} = [\mathbf{w}_1, \dots, \mathbf{w}_K] = (\mu \mathbf{I} + \mathbf{K})^{-1} \mathbf{H} \mathbf{S} \quad (40)$$

where $\mathbf{K} = |s_k|^2 \sum_{i=1}^K \tilde{\mathbf{h}}_i^H \tilde{\mathbf{h}}_i$, $\mathbf{H} = [\tilde{\mathbf{h}}_1^H, \dots, \tilde{\mathbf{h}}_K^H]$ and $\mathbf{S} = \text{diag}([\sqrt{p_1} s_1, \dots, \sqrt{p_K} s_K])$. We have $\text{tr}(\hat{\mathbf{W}} \hat{\mathbf{W}}^H) = \sum_{k=1}^K \hat{\mathbf{w}}_k^H \hat{\mathbf{w}}_k$ and compute the derivative of the transmit power with respect to μ as

$$\begin{aligned} \frac{\partial}{\partial \mu} \text{tr}(\hat{\mathbf{W}} \hat{\mathbf{W}}^H) &= \text{tr} \left(\left(\frac{\partial}{\partial \mu} (\hat{\mathbf{W}} \hat{\mathbf{W}}^H) \right)^H \frac{\partial \hat{\mathbf{W}}}{\partial \mu} \right) \\ &= -2 \text{tr} \left(\mathbf{P}^H (\mu \mathbf{I} + \mathbf{K})^{-1} \mathbf{P} \right), \end{aligned} \quad (41)$$

which shows that (40) is monotonically decreasing with μ . In the critical case of the power constraint (8b), the optimal solution $\hat{\mu}$ corresponds to its minimum value.

REFERENCES

- [1] F. Liu, Y. Cui, C. Masouros, J. Xu, T. X. Han, Y. C. Eldar, and S. Buzzi, "Integrated sensing and communications: Toward dual-functional wireless networks for 6G and beyond," *IEEE J. Sel. Areas Commun.*, vol. 40, no. 6, pp. 1728–1767, Jun. 2022.
- [2] Y. Xu, G. Gui, H. Gacanin, and F. Adachi, "A survey on resource allocation for 5G heterogeneous networks: Current research, future trends, and challenges," *IEEE Commun. Surv.*, vol. 23, no. 2, pp. 668–695, Feb. 2021.
- [3] G. Sun, Y. Zhang, W. Hao, Z. Zhu, X. Li, and Z. Chu, "Joint beamforming optimization for STAR-RIS aided NOMA ISAC systems," *IEEE Wireless Commun. Lett.*, vol. 13, no. 4, pp. 1009–1013, Apr. 2024.
- [4] R. Liu, M. Li, H. Luo, Q. Liu, and A. L. Swindlehurst, "Integrated sensing and communication with reconfigurable intelligent surfaces: Opportunities, applications, and future directions," *IEEE Wireless Commun.*, vol. 30, no. 1, pp. 50–57, Feb. 2023.
- [5] Q. Xue, C. Ji, S. Ma, J. Guo, Y. Xu, Q. Chen, and W. Zhang, "A survey of beam management for mmWave and THz communications towards 6G," *IEEE Commun. Surv. Tutorials*, pp. 1–1, 2024.
- [6] Z. Zhu, Z. Li, Z. Chu, G. Sun, W. Hao, P. Liu, and I. Lee, "Resource allocation for intelligent reflecting surface assisted wireless powered IoT systems with power splitting," *IEEE Trans. Wireless Commun.*, vol. 21, no. 5, pp. 2987–2998, May, 2022.
- [7] R. Liu, M. Li, Y. Liu, Q. Wu, and Q. Liu, "Joint transmit waveform and passive beamforming design for RIS-aided DFRC systems," *IEEE J. Sel. Top. Signal Process.*, vol. 16, no. 5, pp. 995–1010, Aug. 2022.
- [8] M. Di Renzo, A. Zappone, M. Debbah, M.-S. Alouini, C. Yuen, J. de Rosny, and S. Tretyakov, "Smart radio environments empowered by reconfigurable intelligent surfaces: How it works, state of research, and the road ahead," *IEEE J. Sel. Areas Commun.*, vol. 38, no. 11, pp. 2450–2525, Nov. 2020.
- [9] C. Zhou, Y. Xu, D. Li, C. Huang, C. Yuen, J. Zhou, and G. Yang, "Energy-efficient maximization for RIS-aided MISO symbiotic radio systems," *IEEE Trans. Veh. Tech.*, vol. 72, no. 10, pp. 13689–13694, Oct. 2023.
- [10] Z. Lin, H. Niu, K. An, Y. Wang, G. Zheng, S. Chatzinotas, and Y. Hu, "Refracting RIS-aided hybrid satellite-terrestrial relay networks: Joint beamforming design and optimization," *IEEE Trans. Aerosp. Electron. Syst.*, vol. 58, no. 4, pp. 3717–3724, Aug. 2022.
- [11] Z. Chu, Z. Zhu, X. Li, F. Zhou, L. Zhen, and N. Al-Dhahir, "Resource allocation for IRS-assisted wireless-powered FDMA IoT networks," *IEEE Internet Things J.*, vol. 9, no. 11, pp. 8774–8785, Jun. 2022.
- [12] Z. Zhu, Z. Li, Z. Chu, Q. Wu, J. Liang, Y. Xiao, P. Liu, and I. Lee, "Intelligent reflecting surface-assisted wireless powered heterogeneous networks," *IEEE Trans. Wireless Commun.*, vol. 22, no. 12, pp. 9881–9892, Dec. 2023.
- [13] W. Hao, G. Sun, M. Zeng, Z. Chu, Z. Zhu, O. A. Dobre, and P. Xiao, "Robust design for intelligent reflecting surface-assisted MIMO-OFDMA teraHertz IoT networks," *IEEE Internet Things J.*, vol. 8, no. 16, pp. 13052–13064, Aug. 2021.
- [14] W. Hao, J. Li, G. Sun, M. Zeng, and O. A. Dobre, "Securing reconfigurable intelligent surface-aided cell-free networks," *IEEE Trans. Inf. Forensics. Secur.*, vol. 17, pp. 3720–3733, Oct. 2022.
- [15] H. Liu, G. Li, X. Li, Y. Liu, G. Huang, and Z. Ding, "Effective capacity analysis of STAR-RIS-assisted NOMA networks," *IEEE Wireless Commun. Lett.*, vol. 11, no. 9, pp. 1930–1934, Sep. 2022.
- [16] X. Li, Z. Li, Z. Zhu, D. Zhang, L. Liu, and M. Atiquzzaman, "Secrecy rate maximization for intelligent reflecting surface assisted MIMO systems in vehicular networks," *IEEE Internet Things J.*, pp. 1–1, Early Access, 2023.
- [17] Y. Pei, X. Yue, W. Yi, Y. Liu, X. Li, and Z. Ding, "Secrecy outage probability analysis for downlink RIS-NOMA networks with on-off control," *IEEE Trans. Veh. Tech.*, vol. 72, no. 9, pp. 11772–11786, Sep. 2023.
- [18] J. Xu, Z. Zhu, Z. Chu, H. Niu, P. Xiao, and I. Lee, "Sum secrecy rate maximization for irs-aided multi-cluster mimo-noma terahertz systems," *IEEE Trans. Inform. Foren. Sec.*, vol. 18, pp. 4463–4474, July 2023.
- [19] X. Li, J. Zhang, C. Han, W. Hao, M. Zeng, Z. Zhu, and H. Wang, "Reliability and security of CR-STAR-RIS-NOMA assisted IoT networks," *IEEE Internet Things J.*, pp. 1–1, Early Access, 2023.
- [20] X. Li, Y. Zheng, M. Zeng, Y. Liu, and O. A. Dobre, "Enhancing secrecy performance for STAR-RIS NOMA networks," *IEEE Trans. Veh. Tech.*, vol. 72, no. 2, pp. 2684–2688, Feb. 2023.
- [21] X. Li, Z. Tian, W. He, G. Chen, M. C. Gursoy, S. Mumtaz, and A. Nallanathan, "Covert communication of STAR-RIS aided NOMA networks," *IEEE Trans. Veh. Techn.*, pp. 1–6, Early Access, 2024.

- [22] X. Yue, M. Song, C. Ouyang, Y. Liu, T. Li, and T. Hou, "Exploiting active RIS in NOMA networks with hardware impairments," *IEEE Trans. Veh. Tech.*, pp. 1–16, Early Access, 2024.
- [23] F. Liu, C. Masouros, A. Li, H. Sun, and L. Hanzo, "MU-MIMO communications with MIMO radar: From co-existence to joint transmission," *IEEE Trans. Wireless Commun.*, vol. 17, no. 4, pp. 2755–2770, Feb. 2018.
- [24] F. Dong, W. Wang, Z. Hu, and T. Hui, "Low-complexity beamformer design for joint radar and communications systems," *IEEE Commun. Lett.*, vol. 25, no. 1, pp. 259–263, Jan. 2021.
- [25] X. Wang, Z. Fei, Z. Zheng, and J. Guo, "Joint waveform design and passive beamforming for RIS-assisted dual-functional radar-communication system," *IEEE Trans. Veh. Technol.*, vol. 70, no. 5, pp. 5131–5136, May 2021.
- [26] J. Xu, D. Li, Z. Zhu, Z. Yang, N. Zhao, and D. Niyato, "Anti-jamming design for integrated sensing and communication via aerial IRS," *IEEE Trans. Commun.*, pp. 1–1, Early Access, 2024.
- [27] X. Hu, C. Liu, M. Peng, and C. Zhong, "IRS-based integrated location sensing and communication for mmWave SIMO systems," *IEEE Trans. Wireless Commun.*, vol. 22, no. 6, pp. 4132–4145, Jun. 2023.
- [28] A. Magbool, V. Kumar, Q. Wu, M. D. Renzo, and M. F. Flanagan, "A survey on integrated sensing and communication with intelligent metasurfaces: Trends, challenges, and opportunities," Jan. 2024.
- [29] H. Wang, P. Xiao, and X. Li, "Channel parameter estimation of mmwave MIMO system in urban traffic scene: A training channel-based method," *IEEE Trans. Intell. Transp. Syst.*, vol. 25, no. 1, pp. 754–762, Jan. 2024.
- [30] H. Wang, L. Xu, Z. Yan, and T. A. Gulliver, "Low-complexity MIMO-FBMC sparse channel parameter estimation for industrial big data communications," *IEEE Trans. Ind. Inform.*, vol. 17, no. 5, pp. 3422–3430, May 2021.
- [31] H. Wang, X. Li, R. H. Jhaveri, T. R. Gadekallu, M. Zhu, T. A. Ahanger, and S. A. Khowaja, "Sparse bayesian learning based channel estimation in fbmc/oqam industrial IoT networks," *Comput. Commun.*, vol. 176, pp. 40–45, Aug. 2021.
- [32] C. Pan, G. Zhou, K. Zhi, S. Hong, T. Wu, Y. Pan, H. Ren, M. D. Renzo, A. Lee Swindlehurst, R. Zhang, and A. Y. Zhang, "An overview of signal processing techniques for RIS/IRS-aided wireless systems," *IEEE J. Sel. Top. Signal Process.*, vol. 16, no. 5, pp. 883–917, Aug. 2022.
- [33] M. R. Akdeniz, Y. Liu, M. K. Samimi, S. Sun, S. Rangan, T. S. Rappaport, and E. Erkip, "Millimeter wave channel modeling and cellular capacity evaluation," *IEEE J. Sel. Areas Commun.*, vol. 32, no. 6, pp. 1164–1179, Jun. 2014.
- [34] K. Shen and W. Yu, "Fractional programming for communication systems part I: Power control and beamforming," *IEEE Trans. Signal Process.*, vol. 66, no. 10, pp. 2616–2630, May 2018.
- [35] P. J. Rousseeuw and G. Molenberghs, "Transformation of non positive semidefinite correlation matrices," *Commun. Statist. - Theory Methods*, vol. 22, no. 4, pp. 965–984, Taylor & Francis. Press, 1993.
- [36] J. Song, P. Babu, and D. P. Palomar, "Sequence design to minimize the weighted integrated and peak sidelobe levels," *IEEE Trans. Signal Process.*, vol. 64, no. 8, pp. 2051–2064, Apr. 2016.
- [37] K. Alhujaili, V. Monga, and M. Rangaswamy, "Transmit MIMO radar beampattern design via optimization on the complex circle manifold," *IEEE Trans. Signal Process.*, vol. 67, no. 13, pp. 3561–3575, Jul. 2019.
- [38] X. Yu, J.-C. Shen, J. Zhang, and K. B. Letaief, "Alternating minimization algorithms for hybrid precoding in millimeter wave MIMO systems," *IEEE J. Sel. Topics Signal Process.*, vol. 10, no. 3, pp. 485–500, Apr. 2016.
- [39] I. Bekkerman and J. Tabrikian, "Target detection and localization using MIMO radars and sonars," *IEEE Trans. Signal Process.*, vol. 54, no. 10, pp. 3873–3883, Oct. 2006.



Zhengyu Zhu (Senior Member, IEEE) received the Ph.D. degree in information engineering from Zhengzhou University, Zhengzhou, China, in 2017. From October 2013 to October 2015, he visited the Communication and Intelligent System Laboratory, Korea University, Seoul, South Korea, to conduct a collaborative research as a Visiting Student. He is currently an associate professor with Zhengzhou University. He served as an Associate Editor for the IEEE SYSTEMS JOURNAL, JOURNAL OF COMMUNICATIONS AND NETWORKS, the PHYSICAL COMMUNICATIONS. His research interests include information theory and signal processing for wireless communications such as B5G/6G, Intelligent reflecting surface, the Internet of Things, machine learning, millimeter wave communication, UAV communication, physical layer security, convex optimization techniques, and energy harvesting communication systems.

His research interests include information theory and signal processing for wireless communications such as B5G/6G, Intelligent reflecting surface, the Internet of Things, machine learning, millimeter wave communication, UAV communication, physical layer security, convex optimization techniques, and energy harvesting communication systems.



Zheng Li (Student Member, IEEE) received M.S. degree in communication engineering from Zhengzhou University, China, in 2023. He is currently pursuing the Ph.D degree with the School of Electronic and Information Engineering, Zhengzhou University. His research interests include Intelligent reflecting surface, wireless power communication network, integrated sensing and communication, and array signal processing.



Zheng Chu (Member, IEEE) received the M.Sc. and Ph.D. degrees from Newcastle University, Newcastle upon Tyne, U.K., in 2012 and 2016, respectively. Currently, he is an Assistant Professor with the University of Nottingham Ningbo China. Prior to this, he worked with Middlesex University, London, U.K., from 2016 to 2017, and 6GIC, University of Surrey, Guildford, U.K., from 2017 to 2023. His current research interests include smart radio environments/smart reflecting surface, 5G/6G communication networks, Internet of Things networks, artificial-intelligence-driven future networks, wireless information security, and wireless powered networks. Dr. Chu received the Exemplary Reviewer for the IEEE TRANSACTIONS ON COMMUNICATIONS in 2022. He has been recognized as High-Level Talent by Ningbo Municipal Government, China, in 2023.

artificial-intelligence-driven future networks, wireless information security, and wireless powered networks. Dr. Chu received the Exemplary Reviewer for the IEEE TRANSACTIONS ON COMMUNICATIONS in 2022. He has been recognized as High-Level Talent by Ningbo Municipal Government, China, in 2023.



Yingying Guan (Student Member, IEEE) received the M.S. degree in communication and information systems from Northeastern University, Shenyang, China, in 2017. She is currently working toward the Ph.D. degree with Northeastern University, Shenyang, China. From 2019 to 2020, she was a Visiting Researcher at University of Exeter, Exeter, U.K. Her current research interests include network slicing, edge computing, and resource management.



Qingqing Wu (Senior Member, IEEE) is an Associate Professor with Shanghai Jiao Tong University. His current research interest includes intelligent reflecting surface (IRS), unmanned aerial vehicle (UAV) communications, and MIMO transceiver design. He has coauthored more than 100 IEEE journal papers with 29 ESI highly cited papers and 9 ESI hot papers, which have received more than 20,000 Google citations. He was listed as the Clarivate ESI Highly Cited Researcher in 2022 and 2021, the Most Influential Scholar Award in AI-2000 by Aminer in 2021 and World's Top 2 %.

He was the recipient of the IEEE Communications Society Fred Ellersick Prize, IEEE Best Tutorial Paper Award in 2023, Asia-Pacific Best Young Researcher Award and Outstanding Paper Award in 2022, Young Author Best Paper Award in 2021, the Outstanding Ph.D. Thesis Award of China Institute of Communications in 2017, the IEEE ICC Best Paper Award in 2021, and IEEE WCSP Best Paper Award in 2015. He was the Exemplary Editor of IEEE Communications Letters in 2019 and the Exemplary Reviewer of several IEEE journals. He serves as an Associate Editor for IEEE Transactions on Communications, IEEE Communications Letters, IEEE Wireless Communications Letters. He is the Lead Guest Editor for IEEE Journal on Selected Areas in Communications. He is the workshop co-chair for IEEE ICC 2019-2023 and IEEE GLOBECOM 2020. He serves as the Workshops and Symposia Officer of Reconfigurable Intelligent Surfaces Emerging Technology Initiative and Research Blog Officer of Aerial Communications Emerging Technology Initiative. He is the IEEE Communications Society Young Professional Chair in Asia Pacific Region



Pei Xiao (Senior Member, IEEE) is a Professor in Wireless Communications in the Institute for Communication Systems (ICS) at University of Surrey. He is currently the technical manager of 5GIC/6GIC, leading area, the research team in the new physical layer work and coordinating/supervising research activities across all the work areas (<https://www.surrey.ac.uk/institute-communication-systems/5g-6g-innovation-centre>). Prior to this, he worked at Newcastle University and Queen's

University Belfast. He also held positions at Nokia Networks in Finland. He has published extensively in the fields of communication theory, RF and antenna design, signal processing for wireless communications, and is an inventor on over 15 recent patents addressing bottleneck problems in 5G/6G systems.



Marco Di Renzo (Fellow, IEEE) received the Laurea (cum laude) and Ph.D. degrees in electrical engineering from the University of L'Aquila, Italy, in 2003 and 2007, respectively, and the Habilitation Diriger des Recherches (Doctor of Science) degree from University Paris-Sud (currently Paris-Saclay University), France, in 2013. Currently, he is a CNRS Research Director (Professor) and the Head of the Intelligent Physical Communications Group, Laboratory of Signals and Systems (L2S), CNRS, CentraleSupélec, Paris-Saclay University,

Paris, France. Also, he is an elected member of the L2S Board Council and a member of the L2S Management Committee. At Paris-Saclay University, he serves as the Coordinator of the Communications and Networks Research Area of the Laboratory of Excellence DigiCosme, a member of the Admission and Evaluation Committee of the Ph.D. School on Information and Communication Technologies, and a member of the Evaluation Committee of the Graduate School in Computer Science. He is a Founding Member and the Academic Vice Chair of the Industry Specification Group (ISG) on Reconfigurable Intelligent Surfaces (RIS) within the European Telecommunications Standards Institute (ETSI), where he serves as the Rapporteur for the work item on communication models, channel models, and evaluation methodologies. He is a fellow of the IET and AAIA; an Ordinary Member of the European Academy of Sciences and Arts, an Ordinary Member of the Academia Europaea; and a Highly Cited Researcher. Also, he holds the 2023 France-Nokia Chair of Excellence in ICT. He was a Fulbright Fellow with The City University of New York, USA, a Nokia Foundation Visiting Professor, and a Royal Academy of Engineering Distinguished Visiting Fellow. His recent research awards include the 2021 EURASIP Best Paper Award, the 2022 IEEE COMSOC Outstanding Paper Award, the 2022 Michel Monpetit Prize conferred by the French Academy of Sciences, the 2023 EURASIP Best Paper Award, the 2023 IEEE ICC Best Paper Award (wireless), the 2023 IEEE COMSOC Fred W. Ellersick Prize, the 2023 IEEE COMSOC Heinrich Hertz Award, and the 2023 IEEE VTS Jame Evans Avant Grade Award. He served as the Editor-in-Chief for IEEE COMMUNICATIONS LETTERS (2019–2023). He is also serving in the Advisory Board.



Inkyu Lee (Fellow, IEEE) received the B.S. degree (Hons.) in control and instrumentation engineering from Seoul National University, Seoul, South Korea, in 1990, and the M.S. and Ph.D. degrees in electrical engineering from Stanford University, Stanford, CA, USA, in 1992 and 1995, respectively. From 1995 to 2002, he was a member of the Technical Staff with Bell Laboratories, Lucent Technologies, Murray Hill, NJ, USA, where he studied high-speed wireless system designs. Since 2002, he has been with Korea University, Seoul, where he is currently

a Professor with the School of Electrical Engineering. He has also served as the Department Head for the School of Electrical Engineering, Korea University, from 2019 to 2021. In 2009, he was a Visiting Professor with the University of Southern California, Los Angeles, CA, USA. He has authored or coauthored more than 190 journal articles in IEEE publications and holds 30 U.S. patents granted or pending. His research interests include digital communications, signal processing, and coding techniques applied for next-generation wireless systems. Dr. Lee was a recipient of the IT Young Engineer Award at the IEEE/IEEK Joint Award in 2006, the Best Paper Award at the Asia-Pacific Conference on Communications in 2006, the IEEE Vehicular Technology Conference in 2009, the IEEE International Symposium on Intelligent Signal Processing and Communication Systems in 2013, the Best Research Award from the Korean Institute of Communications and Information Sciences in 2011, the Best Young Engineer Award from the National Academy of Engineering of Korea in 2013, and the Korea Engineering Award from the National Research Foundation of Korea in 2017. He has served as an Associate Editor for the IEEE TRANSACTIONS ON COMMUNICATIONS from 2001 to 2011 and the IEEE TRANSACTIONS ON WIRELESS COMMUNICATIONS from 2007 to 2011. In addition, he was a Chief Guest Editor for the IEEE JOURNAL ON SELECTED AREAS IN COMMUNICATIONS (Special Issue on 4G Wireless Systems) in 2006. He currently serves as the Co-Editor-in-Chief for the Journal of Communications and Networks. He has been elected as a member of the National Academy of Engineering of Korea in 2015, and is currently a Distinguished Lecturer of IEEE.